Coplanar-Waveguide-Based Terahertz Hot-Electron-Bolometer Mixers—Improved Embedding Circuit Description

Paolo Focardi, Andrea Neto, and William R. McGrath, *Member, IEEE*

***Abstract*—Series-fed coplanar-waveguide embedding circuits have been recently developed for terahertz mixers using, in particular, superconducting devices as sensors. Although these mixers show promising performance, they usually also show a considerable downward shift in the resonating frequency when compared with calculations using simplified models. This effect is basically caused by parasitics due to the extremely small details (in terms of wavelength) of the device and to the connection of the remaining circuitry (i.e., RF filter). In this paper, we present an improved equivalent-network model of such devices that agrees with measured results. We first propose a method to calculate the characteristic impedance and propagation constant of the coplanar waveguide, etched between two semi-infinite media, which connect the receiving slot antennas to the superconducting device. In the formulation, we take into account, for the first time, the radiation power leakage. We then describe the procedure to calculate the reactances due to the detailed geometry of the mixer device and circuit and we correct the input impedance, calculated with a commonly used simplified network. Finally, by comparing our results with a complete set of measured data, for seven mixers in the range between 500 GHz–3 THz, we analyze the features of our model and propose further improvements. Useful guidelines for designing terahertz mixer circuits are also given.**

***Index Terms*—Characteristic impedance, coplanar waveguide, CPW transitions, hot electron bolometer, leaky waves, slot antennas.**

I. Introduction

SLOT antennas coupled to coplanar waveguides (CPWs) are being developed for quasi-optical single-pixel heterodyne detectors for use in atmospheric and astronomical instruments in the submillimeter-wave/terahertz-frequency range. Hot electron bolometer (HEB) mixers [1], [2], for example, are often used at terahertz frequencies in such circuits placed at the focus of a dielectric lens [3], [4]. HEB receivers are already finding use up to 1 THz on ground-based radiotelescopes [5], and similar receivers are being developed for frequencies up to 2 THz for the European Space Agency (ESA)/National Aeronautics and Space Administration (NASA) Herschel Space Observatory mission, and up to 3 THz for NASA's Stratospheric Observatory for Infrared Astronomy (SOFIA) Aircraft Observatory facility.

Manuscript received September 2, 2001; revised November 14, 2001. This work was supported by a contract from the National Aeronautics and Space Administration.

P. Focardi and W. R. McGrath are with the Microwave Experiment Systems and Technology Section, Jet Propulsion Laboratory, California Institute of Technology, Pasadena, CA 91109 USA (e-mail: paolo.focardi@jpl.nasa.gov; william.r.mcgrath@jpl.nasa.gov).

A. Neto is with FEL–TNO, Den Haag, The Netherlands (e-mail: neto@fel.tno.nl).

Digital Object Identifier 10.1109/TMTT.2002.803448.

The prediction of the radiation pattern (up to 500 GHz) and resonating frequency (up to 100 GHz) for these mixer circuits has been found to be accurate, with respect to measurements, using a simplified network [6]. However, when the device is operated well into the terahertz regime (up to 2.5 THz), the measured resonant frequency (i.e., frequency of the peak response of the detector) is often significantly lower than that calculated with simple models [2], [7]. This leads to significant increases (up to a factor of two) in mixer noise due to the reduction in coupled signal power at the desired terahertz frequency. Thus, as previously reported [7], the accurate characterization of the entire mixer embedding circuit, including the parasitics associated with the geometry of the device, is needed to correctly design the circuit. Even though the geometry of these antennas, CPW lines, and devices is relatively simple, accurately simulating their performance in a terahertz circuit is not a straightforward matter. To the knowledge of the authors, there are no commercial software tools to tackle this problem. It becomes even more difficult to analyze when the lens effect also has to be included [6]. A brute force approach based on a method of moments (MoM) analysis of the overall planar structure can be used, but since the device dimensions can be of the order of $\lambda_0/1000$, the numerical effort required for an accurate analysis becomes almost prohibitive, even for a single antenna. In [8], a dedicated MoM scheme for this kind of structure has been presented.

In this paper, an equivalent network is presented that significantly improves the one presented in [6], though the lens effect is not included in order to concentrate attention to the feed mechanism. The model is improved in the sense that the radiation leakage is accounted for in the calculation of the transmission-line parameters. Additionally, the transition between the CPW and bolometer is characterized via analytically evaluated lumped reactances. The emphasis is given to the physical interpretation rather than to the numerical solution (as in [8]) since this is what will be useful in future designs. In Section II, we first briefly describe the geometry of the detectors and circuits. In Section III, the formulation to calculate the parameters of the equivalent network is then presented. First, we derive the expression of the propagation constant and characteristic admittance of the CPW. These are both complex due to the fact that the propagating mode is a leaky one. Before this study, the quasi-static approximations for these parameters were too inaccurate to correctly predict the actual performance of the circuits under investigation. The work in [9] accounts for a complex propagation constant in coplanar lines. However, in [9], the attenuation was associated with losses in the conductor and di-

electric rather than with the radiation effect, which appears to be dominant in the case investigated in this paper.

A recent investigation [10] presents a direct integration method for the Green's function (GF) of a microstrip. In [11], the method has been applied to slots etched between two semi-infinite dielectrics and provides, analytically in that case, the GF of a gap-excited slot placed between two different homogeneous dielectrics. Here, the procedure is extended to CPWs in order to derive the circuit parameters mentioned above. We then present a procedure that characterizes the strong reactive contributions associated with the transition between the bolometer and CPW. The lumped reactances we obtain are connected to the equivalent network that represents the overall antenna+detector circuit. This circuit is composed of the CPW equivalent transmission lines and the active impedance of the slots; i.e., the impedance of each of the two slots with the mutual coupling taken into account. In Section IV, comparisons with measurements of submillimeter-wave bolometric receivers show that the observed downward shift of the resonant frequency can be explained by: 1) the reactances associated with both the "crowding" of the RF current and the fringing fields in the transition between the bolometer and the CPW (see Fig. 2) and 2) the phase shift caused by the imaginary part of the impedance of the RF band-stop filter used in the dc/IF line. Finally, in Section V, some guidelines for future designs are provided, while in Section VI, conclusions are drawn.

II. Receiver Layout

The mixer circuit is located at the second focus on the back side of a silicon elliptical lens. Since the reflections due to the dielectric lens can be introduced separately, as discussed in [6], we assume the circuit under investigation to be located at the interface between two semi-infinite half spaces ($\epsilon_{r1} = 1$ and $\epsilon_{r2} = 11.7$). The spectral response and, hence, the center frequency of HEB mixers with six different twin-slot antenna designs, have been previously measured with a Fourier-transform spectrometer (FTS) [7]. The antenna slot lengths ranged from 26 up to 152 μm. Fig. 1 shows a scanning electron microscope (SEM) photograph of a 2.5-THz HEB mixer. The submicrometer-sized HEB device (i.e., "microbridge" in this figure) is connected to the twin slot antennas via a CPW transmission line [1]. On the right-hand side, the RF band-stop filter structure (a total of eight high- and low-impedance sections were used) is located. Fig. 2 shows a detail of the transition between the CPW and bolometer. The length of the transition region L and the width of the bolometer w_b are highlighted in this figure. The modeling of this structure could be performed with a full-wave MoM analysis, as described in [8]. However, in this paper, we present an equivalent-network model for the overall mixer embedding circuit. The first simplified equivalent network is shown in Fig. 3. The active slot impedances Z_{sa} are obtained by means of MoM simulations restricted to the receiving slots alone, while $R_{\rm bol}$, Z_0, and V_s represent, respectively, the nominal dc impedance of the bolometer, characteristic impedance of the CPW, and equivalent voltage source of the receiving antenna.

In Section III, the transmission-line parameters are calculated, taking into account, for the first time, the power leakage

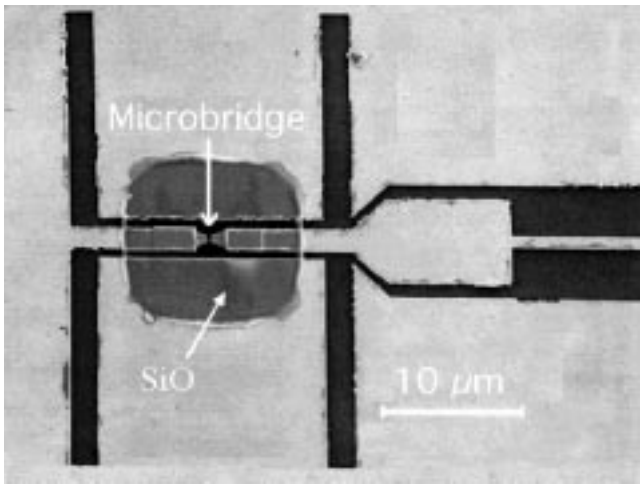

Fig. 1. SEM photograph of an HEB mixer embedding circuit. The superconducting microbridge is located at the center and coupled to the twin-slot antenna via CPW lines.

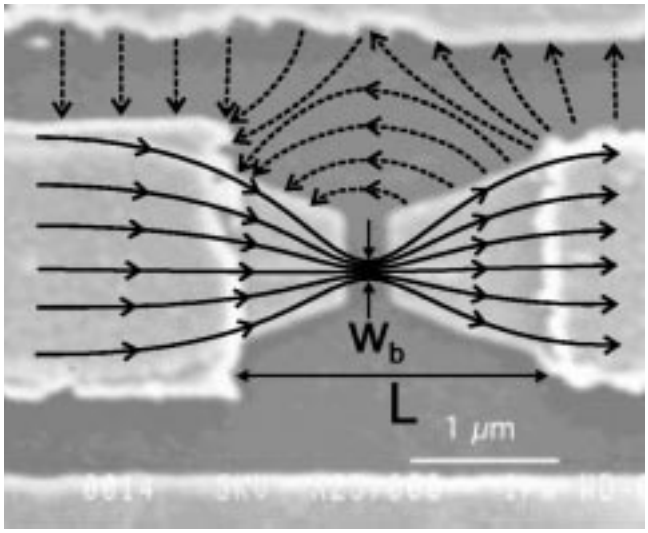

Fig. 2. Bolometer detail of a 2.5-THz design with a schematic representation of the electric field (dashed line) and RF current path (solid line).

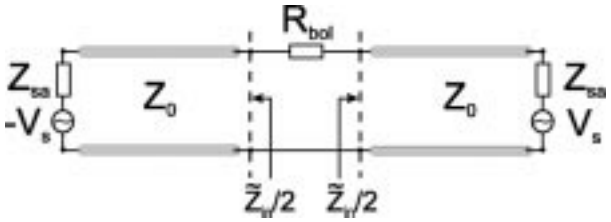

Fig. 3. Simplified equivalent network of the terahertz mixer circuit, which includes the active slot impedance and equivalent transmission lines.

in the two dielectrics. With the simplified equivalent network of Fig. 3, we may then estimate the equivalent series load $\tilde{Z}_{\rm in}$ seen by the bolometer. However, $\tilde{Z}_{\rm in}$ must be modified to account for the reactances due the field deformations shown in Fig. 2, which are associated with the CPW-to-bolometer transition. Analytical expressions for these reactances are also presented in Section III. Finally, as will be discussed in Section IV,

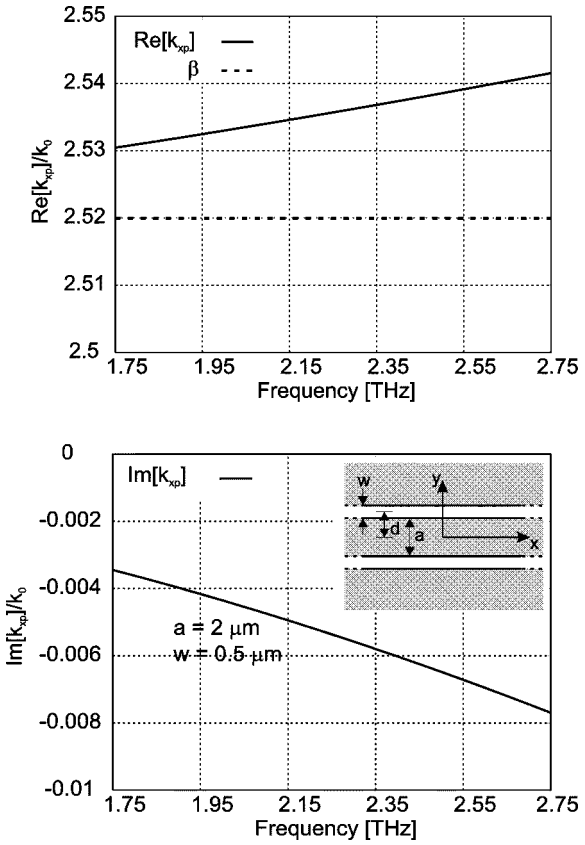

Fig. 4. Real and imaginary parts of the propagation constant for a CPW with $a = 2\ \mu$m and $w = 0.5\ \mu$m. Both graphs are normalized to the free-space wavenumber. The real part also shows a comparison with the value of β from (1) (dashed line).

the effects of the RF filter must also be included to completely characterize $\tilde{Z}_{\rm in}$.

III. Equivalent-Network Parameters

The parameters of the CPW transmission line have been obtained using the formalism that was presented in [11] for the case of a single slot etched in a perfect electric conductor between two semi-infinite dielectrics. In this paper, the same formulation is extended to the case of an infinitely extended CPW whose geometry is shown in the inset of Fig. 4.

A. Propagation Constant

The quasi-static approximation of the propagation constant is $\beta = \sqrt{(k_1^2 + k_2^2)/2}$ [13], where $k_i = k_0\sqrt{\epsilon_{ri}}$ $(i = 1, 2)$ is the wavenumber in each semi-infinite dielectric (air and silicon) and k_0 is the free-space wavenumber. Accordingly, the propagating mode is fast for the denser medium (i.e., silicon) and the mode is leaky. Starting from β, as shown in Appendix A, the complex propagation constant can be expressed as

$$k_{xp} = \beta - \frac{\mathbb{D}(\beta)}{\mathbb{D}'(\beta)}. \tag{1}$$

The expression of $\mathbb{D}(k_x)$ is

$$\mathbb{D}(k_x) = \sum_{i=1}^{2} \frac{4\left(k_x^2 - k_i^2\right)}{wk_0\zeta_0} \left[\int_{2d-(w/2)}^{2d+(w/2)} \frac{H_0^2\left(\tilde{k}_i|y|\right)}{\sqrt{1 - \dfrac{4(2d-y)^2}{w^2}}}\, dy - 2\int_0^{w/2} \frac{H_0^2\left(\tilde{k}_i|y|\right)}{\sqrt{1 - \dfrac{4y^2}{w^2}}}\, dy \right] \tag{2}$$

where $\tilde{k}_i = \sqrt{k_i^2 - k_x^2}$, ζ_0 is the free-space characteristic impedance and the index $i = 1, 2$ represent the contribution in each semi-infinite dielectric. Also, in evaluating k_{xp}, $\mathrm{Im}[\sqrt{k_i^2 - \beta^2}] < 0$. Despite the cumbersome expression, the evaluation of $\mathbb{D}(k_x)$ is extremely efficient numerically and the evaluation of $\mathbb{D}'(k_x)$ is straightforward from (2).

In Fig. 4, an example of the propagation constant is shown for a CPW with $a = 2\ \mu$m and $w = 0.5\ \mu$m (these are typical values for a terahertz circuit), as sketched in the inset. Both graphs are normalized to the free-space wavenumber. In the upper graph, the real part of k_{xp} is shown, compared with the value of β (dashed line) from (1). As the frequency increases, the value of $\mathrm{Re}[k_{xp}]$ tends asymptotically to the value of the propagation constant in the denser medium (silicon). In the lower graph, the attenuation constant ($\mathrm{Im}[k_{xp}]$) is seen to change significantly over the frequency range of 1 THz.

B. Characteristic Admittance

The definition of the characteristic admittance for a leaky line is a "hot topic" and has been the subject of recent investigations; of particular promise is the one in [12]. In this paper, we define the characteristic admittance at a specific transverse section as the ratio between current and voltage of the leaky wave launched by a source at finite distance. This avoids some of the ambiguities that arise with a leaky transmission line when the source is assumed to be at infinite distance. Indeed, since the propagating mode is exponentially attenuated in x, for x tending to infinity, the major field contribution on the slot axis are due to fringe currents (that decay as $1/x^2$) rather than to the mode itself [11]. The evaluation of the characteristic admittance is shown in Appendix B and the final expression is

$$Y_0 = \sum_{i=1}^{2} \frac{2k_{xp}}{j\pi k_0\zeta_0 w} \left[\int_{2d-w}^{2d} \frac{H_0^2(\tilde{k}_{ip}|y|)}{\sqrt{1 - \dfrac{4\left(2d - \dfrac{w}{2} - y\right)^2}{w^2}}}\, dy - \int_0^{w} \frac{H_0^2(\tilde{k}_{ip}|y|)}{\sqrt{1 - \dfrac{4\left(\dfrac{w}{2} - y\right)^2}{w^2}}}\, dy \right] \tag{3}$$

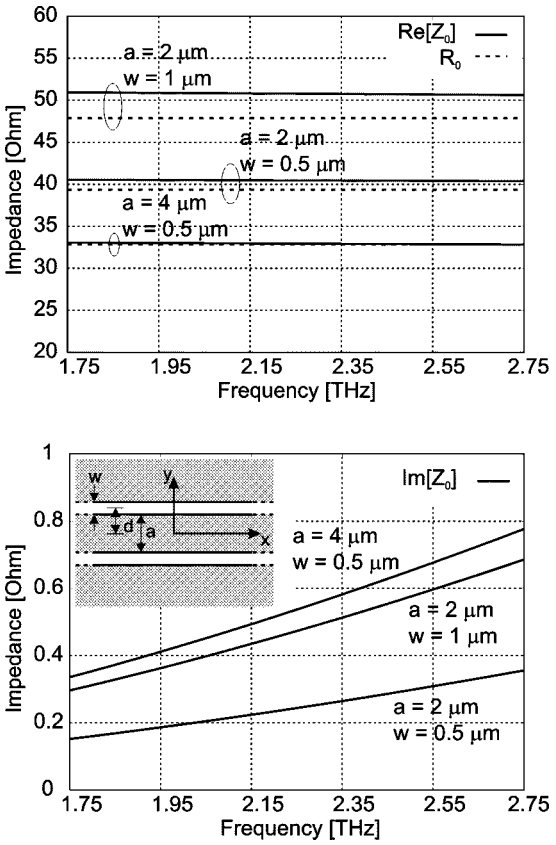

Fig. 5. Real and imaginary part of the CPW characteristic impedance for three different CPW geometries. For the real part, a comparison between the formulation of this paper (solid line) and the quasi- static approximation (dashed line) is shown in the upper graph.

where $\tilde{k}_{ip} = \sqrt{k_i^2 - k_{xp}^2}$ and $\mathrm{Im}[\tilde{k}_{ip}] < 0$ for $i = 1$ and $\mathrm{Im}[\tilde{k}_{ip}] > 0$ for $i = 2$. Equation (3), when compared with previously existing expressions [13], accounts for the frequency dependence and power leakage. It can be demonstrated that this definition is also congruent with the one given by Das in [12], even if it is based on a voltage/current definition rather than on power consideration. In applying the definition given in [12], one should note that, in this case, there is no surface-wave pole contribution to the GF, as we are dealing with grounded homogeneous dielectrics.

In Fig. 5, the characteristic impedance of a CPW with three different geometries is shown, along with the values obtained with the quasi-static approximation formulated in [13]. Equation (3) provides not only the imaginary part, but it can also be seen that the quasi-static formula underestimates the real part of Z_0 when the width of the CPW slots grows with respect to the inner conductor a. In particular, this aspect significantly impacts the simulation results when introducing a transmission-line model of the band-stop filtering structure.

C. Reactances

The equivalent network in Fig. 3 alone provides $\tilde{Z}_{\mathrm{in}}$, which does not account for the electric and magnetic current crowding effects occurring in the transition between the bolometer and CPW. Since the bolometer width is much narrower with respect to the CPW inner conductor, strong reactive energy is concentrated at this transition (see Fig. 2). Our analysis accounts for the effect of the transition by correcting $\tilde{Z}_{\mathrm{in}}$ via the introduction of two lumped reactances related to the lengths and widths involved in the transition. These two reactances are combined to represent a realistic model of the transition. In this way, we can then calculate Z_{in}, which is the actual embedding circuit series impedance seen by the bolometer.

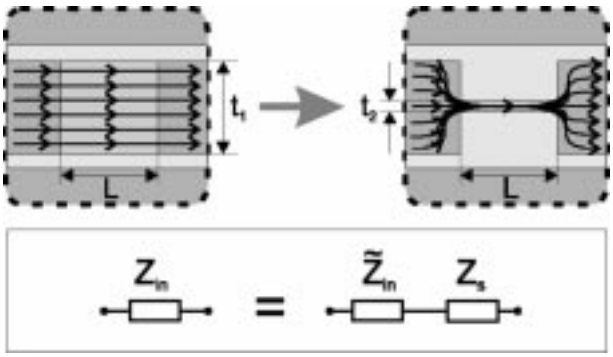

Fig. 6. Electric current crowding effect with the relevant dimensions indicated. In the upper part of this figure, the electric current is sketched. In the lower part of the figure, the connection of Z_s to the equivalent circuit is represented.

With reference to Fig. 6, the effect on the input impedance of the electric current crowding associated with an inner conductor reduction ($t_1 \rightarrow t_2$) can be represented as a series inductive impedance Z_s. An infinite slot, whose width is equal to L, is the canonical problem that best fits the geometry in Fig. 6. The growth of inductive energy associated with the reduction of the inner conductor from t_1 to t_2 is assumed to be the same as that occurring in the selected canonical problem when the dimension of the source region is reduced accordingly. Z_s is derived in [14], and its explicit expression is

$$Z_s = Z(t_2) - Z(t_1) \tag{4}$$

where

$$Z(t_i) = k_0 L\big[Z_a(t_i) + Z_b(t_i)\big] \tag{5}$$

and

$$Z_a(t_i) = \frac{j\pi\zeta_0}{2t_i^2\left(k_1^2 - k_2^2\right)}\left\{\frac{H_0^2(k_2t_i) - J_0(k_2t_i)}{-j} - \frac{H_0^2(k_1t_i) - J_0(k_1t_i)}{-j} + \frac{2}{\pi}\ln\left(\frac{k_1}{k_2}\right)\right\} \tag{6}$$

$$Z_b(t_i) = \frac{\pi\zeta_0}{2}\left\{\frac{j}{2}\left[-\frac{2}{\pi}\ln(\gamma' t_i) + \frac{3}{\pi}\right] - \frac{j\left[k_1^2\ln\left(\frac{k_1}{2}\right) - k_2^2\ln\left(\frac{k_2}{2}\right)\right]}{\pi\left(k_1^2 - k_2^2\right)}\right\} \tag{7}$$

where $\gamma' = 1.781\cdots = e^{\gamma}$ and γ is the Euler constant. The series impedance Z_s grows linearly with the length L of the

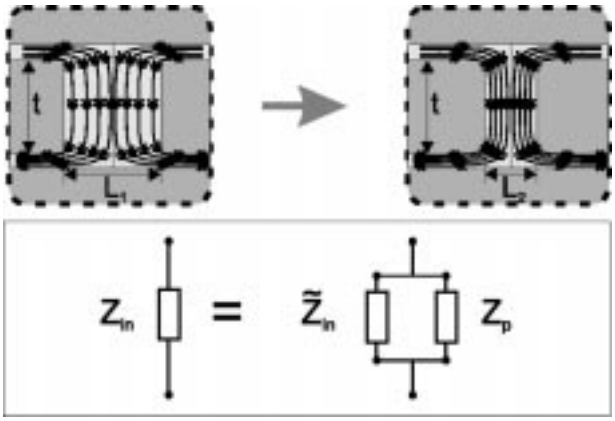

Fig. 7. Magnetic current crowding effect with the relevant dimensions indicated. In the upper part of this figure, the magnetic current is sketched. In the lower part of this figure, the connection of $Z_p = 1/Y_p$ to the equivalent circuit is represented.

transition. It is also proportional to $\ln(t_2)$ as t_2 tends to zero, even though this is not evident from (6) and (7).

With reference to Fig. 7, the effect on the input impedance of the magnetic current crowding associated with shortening the gap length ($L_1 \rightarrow L_2$) can be represented as a parallel capacitive admittance Y_p. An infinite dipole printed between two semi-infinite dielectrics, whose width is equal to t, is the canonical problem that best fits the geometry in Fig. 7. The growth of capacitive energy in the fringing fields associated with a reduction of the gap from L_1 to L_2 is assumed to be the same as that occurring in this selected canonical problem when the dimension of the source region is reduced accordingly. Y_p is derived in [15], and its explicit expression is

$$Y_p = Y(L_2) - Y(L_1) \tag{8}$$

where

$$Y(L_i) = \sum_{n=1}^{2} Y_n(L_i) \tag{9}$$

and

$$Y_n(L_i) = -\frac{jtk_0\epsilon_n}{\pi\zeta_0}\left[\ln\left(\gamma'\frac{k_n}{2}L_i\right) - \frac{3}{2}\right]. \tag{10}$$

The parallel admittance Y_p grows linearly with the width t of the transition. Again, it is proportional to $\ln(L_2)$ as L_2 tends to zero.

In order to account for a more general transition, we can combine the previous reactances in a staircase form, resulting in an equivalent network, as shown in Fig. 8. Note that all the parameters of the network are calculated with the closed-form expressions of (4) and (8), provided that the largest dimensions of the transition are approximately less than $\lambda_{\text{eff}}/20$, where $\lambda_{\text{eff}} = 2\pi/\beta$ and β is as shown in (1).

IV. Numerical Results

The parameters of the twin-slot mixers that have been measured and analyzed are given in Table I, along with the

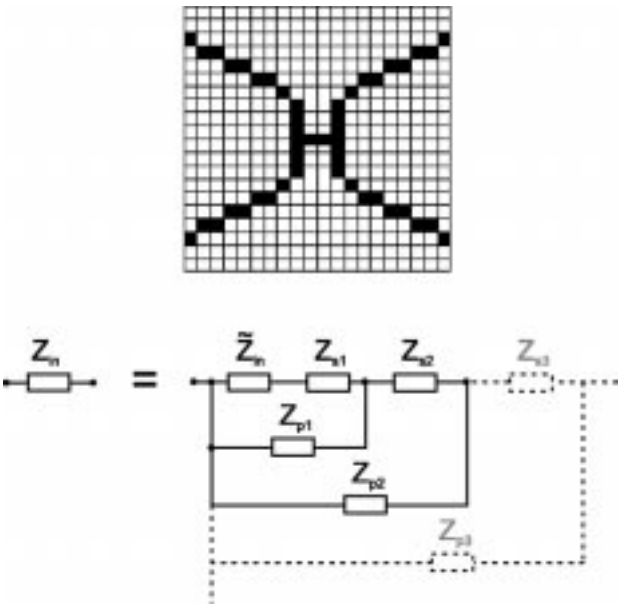

Fig. 8. Example of transition adopted to simulate the actual circuit geometry and of the equivalent network obtained, resorting to a "staircase"-shaped transition using the impedances of (4) and (8) to correct $\tilde{Z}_{\text{in}}$. The layout shown here is representative of the tapered transition region of Mixer No. 1. Each unit represents 0.1 μm.

TABLE I
PARAMETERS OF THE DIFFERENT MIXER CIRCUITS UNDER INVESTIGATION. R_{bol} IS THE HEB DEVICE DC RESISTANCE. REFER TO FIG. 9 FOR THE MEANING OF THE OTHER PARAMETERS

Mixer	L_a (μm)	W_a (μm)	S_a (μm)	a (μm)	b (μm)	R_{bol} T = 4°K	ν_c Measured (THz)
1	26	3	19	3	4	15	2.22
2	33	3	19	3	4	18	2.19
3	36.5	2	19	2	3	18	2.02
4	36.5	2	19	2	3	25	2.01
5	44	4	25	4.5	6	46	1.60
6	48	2.6	25	3	4.4	25	1.71
7	152	8.3	79.2	8	11	32	0.54

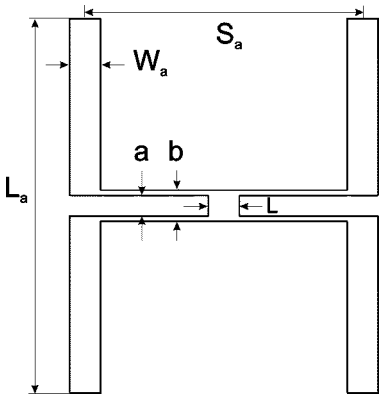

Fig. 9. Schematic layout of physical structure used in the simulations with the relevant dimensions defined.

bolometer device dc resistance and, in Fig. 9, the relevant geometric parameters are indicated. Fig. 10 shows the resonance frequency for the mixers under investigation. The measured results (dashed line with "prism" symbols) are compared with calculated curves that are obtained by using either the simplified network as it is ("plus" symbols) or corrected via the

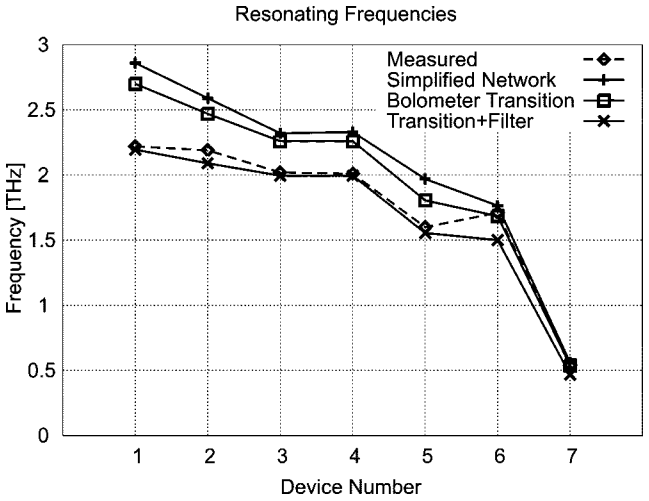

Fig. 10. Summary of measured and calculated resonating frequencies for the seven mixers under analysis.

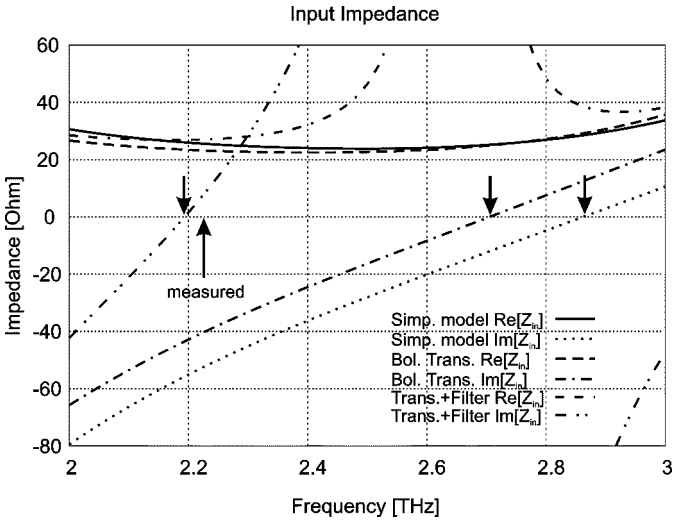

Fig. 11. Input impedance of Mixer No. 1 calculated including: 1) simplified network, 2) simplified network + bolometer transition, and 3) simplified network + bolometer transition + RF filter.

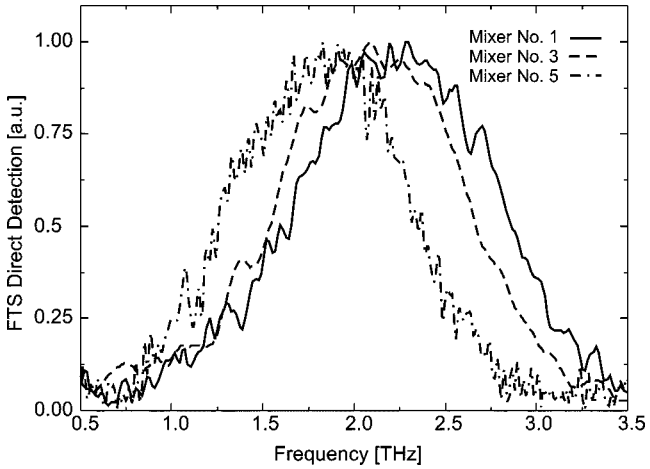

Fig. 12. Measured FTS direct detection response for Mixer No. 1, 3, and 5.

reactive current crowding contributions ("square" symbols). These latter are obtained assuming the flared transition between the bolometer and inner conductor of the CPW, such as in Fig. 8, taking into account the actual dimensions of the mixer embedding circuits observed with a scanning electron microscope. While the series inductance of (4) tends to decrease the resonating frequency of the mixer, the parallel capacitance of (8) tends instead to increase it. However, the overall effect, as shown in Fig. 10 ("square" symbols), is that the resonating frequency decreases, with respect to the simplified model. This means that the inductive part of the reactance we introduced tends to prevail.

The resonating frequency is even more strongly affected by the presence of the filtering structure. This latter has been modeled by simple transmission-line theory, where the relevant parameters are evaluated as in Sections III-A and III-B. Also shown in Fig. 10 are the results ("×" symbols) obtained when the impact of the RF filter is included. It is apparent that the agreement between prediction and measurement is outstanding, except for the case of Mixer No. 6. These results give strong support to our improved equivalent network, considering the extreme challenges associated with fabrication and measurement at 2.5 THz and the fact that the modeling of the filter does not account for the "step" transitions between the high- and low-impedance sections. However, the latter can be considered higher order effects, easily comparable with other phenomena that are not accounted for in this analysis (i.e., internal reflections inside the lens, gluing of the silicon lens to the chip, fabrication tolerances, variation of metal thickness, etc.). Moreover, it is clear, as discussed below, that selecting the resonant frequency from the measured peak of the FTS data is not a straightforward matter.

It is useful to refer to the percentage resonating frequency shift as the difference between the predicted and measured frequency. We may highlight this shift by observing Fig. 11 where the input impedance of Mixer No. 1 is shown. Arrows indicate the resonating frequencies, for measured and predicted results, that occur when the imaginary parts of the impedance cross zero. Improving the simplified network with only the effect of the bolometer–CPW transition decreases the shift from 29% to 22%. By further introducing the effect of the filter, the resonant frequency shift decreases to 1%.

In the past, the observed shift has been attributed to unknown lumped reactive effects associated with the superconducting bolometer itself (i.e., thermal gradients and skin effects). The present analysis attributes the dominant part of the observed shift to the embedding circuit modeled in this paper. From Fig. 11, one can also outline the significant impact of the filter on the real part of the input impedance and the narrowing of the bandwidth due to the several high- and low-impedance sections used in the filter.

In Fig. 12, the FTS direct detection response of Mixer No. 1, 3, and 5 are presented. For the same set of mixers, Fig. 13 shows the predicted coupling efficiency between input and bolometer impedance. The latter are obtained resorting to the following well-known impedance-mismatch expression:

$$\eta = 1 - \left| \frac{R_{\rm bol} - Z_{\rm in}}{R_{\rm bol} + Z_{\rm in}} \right|^2 \tag{11}$$

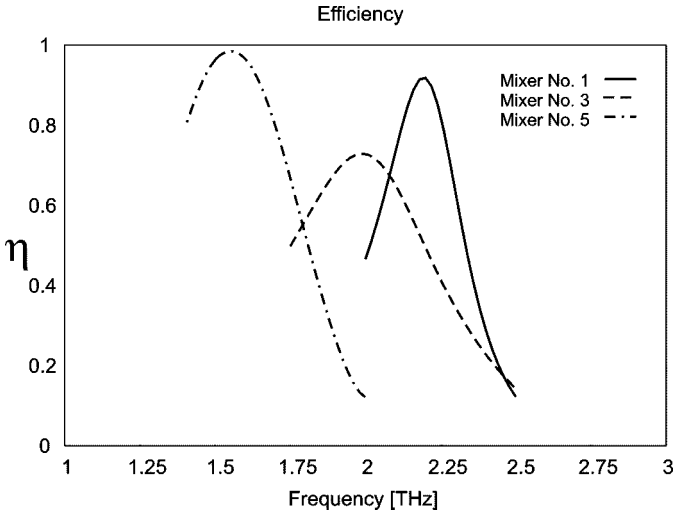

Fig. 13. Calculated coupling efficiency curves for Mixer No. 1, 3, and 5.

where $R_{\rm bol}$ is the resistance of the bolometer and $Z_{\rm in}$ is the series impedance seen by the device in the equivalent circuit. The measured bandwidths appear larger than the calculated ones. This is basically due to the normalization adopted in the FTS curves: these are normalized to the maximum of the peak response, while those in Fig. 13 reflect the calculated mismatch between bolometer and input impedance. The ripples in the measured curve are due to several effects related to the quasi-optical FTS measurement system, particularly the lens internal reflections [6] and thickness of the glue layer holding the chip to the lens.

V. Design Considerations

Based on previous results, some guidelines for future design of CPW-based twin-slot bolometric mixers are now given.

In the past [4], [6], the main constraint in the design of such a mixer has been the overall beam pattern of the antennas+lens system; the emphasis being given to a Gaussian shaped beam and, consequently, good radiation efficiency. This goal was achieved operating the twin-slot antenna at its second resonance. In this way, a low real part of the input impedance for each slot was obtained and a good match to the characteristic impedance of the CPW could be achieved (each one in the order of 40 Ω). More problematic instead was the matching between the bolometer impedance (typically low to obtain a fast response from the device) and the equivalent load represented by the CPW and slot antennas on each side of the bolometer. Moreover, the nonzero reactance, provided by the RF filter, could significantly affect the impedance of the equivalent load of the slot connected to the filter itself. This latter effect and the CPW–bolometer transition play a dominant role in explaining the downward shift of the resonating frequency shown by the mixers under investigation.

As a result of the present investigation, it seems more convenient to operate the slot antennas on their first resonance (half-wavelength instead of a full-wavelength-long slot). Indeed, even though the overall radiation pattern could be slightly affected and different from the theoretical optimum, the input impedance of the radiating slots turns out to be higher (approximately 140 Ω for the real part of Mixer No. 1 at 2.5 THz). In this way, the slot input impedance is more stable and the impact of the imaginary part of the filtering structure is less significant because it is in series to a high impedance.

To further motivate this choice, it is worth mentioning that the previous studies on the beam efficiency [4] were based on physical optics (PO) calculations of the radiation patterns. There are currently ongoing studies that include more sophisticated diffraction mechanisms [16]. The latter could affect the calculation of the optimum beam efficiency for these kind of lenses. Additionally, when the slot antennas are operated on their first resonance, the slot impedance presented to the bolometer via a $\lambda_{\rm eff}/4$-long CPW transmission line is much lower and typically about 20 Ω. This way, a good match of the real part of this impedance with that of the bolometer is straightforward, which results in a nearly optimum efficiency. It is true that, in this configuration, the impact of the lumped reactances associated with the CPW–bolometer transition are more relevant. However, when observing the analytical expressions presented in Section III-C, it is clear that the effect of this transition is negligible if the length of the transition L is reduced to the minimal realizable dimension without resorting to the flared transition of Fig. 2.

VI. Conclusions

In this paper, we have presented an improved model for series-fed CPW embedding circuits that are used in bolometric terahertz receivers. We first calculated the complex propagation constant and characteristic impedance of the weakly leaky mode propagating in the CPW etched between two semi-infinite dielectrics. It is found that, for higher values of the characteristic impedance, the quasi-static approximation is inadequate for an accurate design that aims to match the CPW impedance to the radiating slots or to the bolometer. We have also presented an improved model of the planar transition between the CPW and bolometer.

Using these improvements, we have investigated seven mixers developed for real instrument applications and we have been able to explain the downward shift in the resonating frequency when comparing simplified predictions with the actual measurements. Higher order physical effects that can contribute to the input impedance of the circuit are still not taken into account. In particular, the bolometer impedance is accurately known only in dc and it is not necessarily real at 2.5 THz. Skin effects could have an impact on the overall circuit and other reactances could be associated with the vertical variation of the metal thickness between the CPW inner conductor and superconductive metal of the HEB device. Finally, the transitions between high- and low-impedance sections of the filter should be taken into account.

Nevertheless, the results obtained by our improved equivalent network are outstanding, considering the extreme challenges associated with fabrication and measurement at 2.5 THz.

Appendix A

The transmission line is fed by an x-oriented forcing magnetic field concentrated on $x = 0\,(H_f(x) = \delta(x))$ and constant

on the transverse dimension y. In particular, the forcing magnetic field is supposed to have the same amplitude, but opposite phase, on the two slots of the CPW, in order to be compatible with a propagating mode in the line. The problem is formalized as a continuity of magnetic field integral equation (CMFIE) assuming, as in [11], the separability between transverse and longitudinal space functional dependence of the unknown magnetic currents distributed on the slots. In particular, the transverse electric field is assumed to be well represented by a unique edge singular function defined on each of the two slots. Thus, we can express the magnetic current as

$$M(x, y) = V(x)M_y(y) \tag{12}$$

where

$$M_y(y) = \frac{2}{w\pi}\left[\frac{U_1}{\sqrt{1-\left[\dfrac{2(y+d)}{w}\right]^2}} - \frac{U_2}{\sqrt{1-\left[\dfrac{2(y-d)}{w}\right]^2}}\right]. \tag{13}$$

U_i is the unitary "rect function" of the ith slot and the expression is normalized in such a way that $V(x)$ represents the voltage drop between the inner conductor and the two outer conducting planes. Following the same procedure as in [11], in forcing the CMFIE only on the slot axis, we obtain $V(x)$ as an inverse Fourier transform (FT)

$$V(x) = \frac{1}{2\pi}\int_{-\infty}^{+\infty} \frac{2}{\mathbb{D}(k_x)}\, e^{-jk_x x}\, dk_x \tag{14}$$

where $1/\mathbb{D}(k_x)$ is the CPW magnetic current spectral GF and is expressed as

$$\mathbb{D}(k_x) = \frac{1}{2\pi}\int_{-\infty}^{+\infty} \mathbb{G}_{xx}^{mh}(k_x, k_y) J_0\left(k_y \frac{w}{2}\right) \cdot \left[2j\sin(k_y d)\right]^2 dk_y. \tag{15}$$

In this expression, $J_0(k_y(w/2))$ is the zeroth-order Bessel function. $\mathbb{G}_{xx}^{mh}$ is the xx component of the dyadic spectral GF pertinent to the magnetic field radiated by the magnetic currents in absence of the CPW

$$\mathbb{G}_{\left\{\substack{xx\\xy}\right\}}^{mh}(k_x, k_y) = \sum_{i=1}^{2} \frac{\left\{\substack{k_i^2-k_x^2\\k_x k_y}\right\}}{k_0\zeta_0\sqrt{k_i^2-k_x^2-k_y^2}} \tag{16}$$

where k_0 is the free-space wavenumber, ζ_0 is the free-space characteristic impedance, and the index $i = 1, 2$ represent the contribution of each semi-infinite dielectric. Equating to zero the denominator of the spectral expression for the magnetic currents [$\mathbb{D}(k_x) = 0$ in (14)], a dispersion equation is obtained, which, when numerically solved, defines the propagation constant k_{xp} of the mode supported by the structure. Since the CPW is placed at the interface between two different semi-infinite dielectrics (silicon and air), the propagating mode is fast for the denser (i.e., silicon) medium and the mode is leaky. In order to solve the dispersion equation, it is convenient to re-express (15) in a slightly different form. This is accomplished by first noticing that

$$J_0\left(k_y \frac{w}{2}\right) = \int_{-(w/2)}^{+(w/2)} \frac{2}{w\pi} \frac{e^{jk_y y}}{\sqrt{1-\left(\dfrac{2y}{w}\right)^2}}\, dy \tag{17}$$

and then that the zeroth-order second-kind Hankel function of complex argument can be represented as

$$H_0^2\left(\tilde{k}|\omega|\right) = \frac{1}{\pi}\int_{-\infty}^{+\infty} \frac{e^{-jk_y\omega}}{\sqrt{\tilde{k}^2-k_y^2}}\, dk_y. \tag{18}$$

Finally, substituting (17) and (18) in (15) and inverting the order of the space and spectral integrations, we obtain

$$\mathbb{D}(k_x) = \sum_{i=1}^{2} \frac{4\left(k_x^2-k_i^2\right)}{wk_0\zeta_0}\left[\int_{2d-(w/2)}^{2d+(w/2)} \frac{H_0^2\left(\tilde{k}_i|y|\right)}{\sqrt{1-\dfrac{4(2d-y)^2}{w^2}}}\, dy - 2\int_0^{w/2} \frac{H_0^2\left(\tilde{k}_i|y|\right)}{\sqrt{1-\dfrac{4y^2}{w^2}}}\, dy\right] \tag{19}$$

where $\tilde{k}_i = \sqrt{k_i^2-k_x^2}$. This latter expression of $\mathbb{D}(k_x)$ is extremely efficient for numerical evaluation. Moreover, it does not present any more square-root-type branches in k_y. $\mathbb{D}(k_x)$ is an analytical function of k_x once the branch cuts in the k_x complex plane are selected, as in [11]. Since $k_x = \beta = \sqrt{(k_1^2+k_2^2)/2}$ constitutes the quasi-static expression of the propagation constant, $\mathbb{D}(k_x)$ can be expanded in a power series in terms of β

$$\mathbb{D}(k_x) = \mathbb{D}(\beta) + \mathbb{D}'(\beta)(k_x-\beta) + \cdots. \tag{20}$$

Accordingly, a second-order approximation of the propagation and attenuation constants in the CPW can be derived inverting (20). Thus, the complex wavenumber of the propagating leaky mode results as follows:

$$k_{xp} = \beta - \frac{\mathbb{D}(\beta)}{\mathbb{D}'(\beta)}. \tag{21}$$

Note that, in evaluating k_{xp}, $\mathrm{Im}[\sqrt{k_i^2-\beta^2}] < 0$ for $i = 1, 2$. Finally, the evaluation of $\mathbb{D}'(k_x)$ is straightforward from (19).

APPENDIX B

The characteristic admittance of the CPW is defined as the ratio between current and voltage associated with the modal propagation (k_{xp}). The total voltage along the CPW has been introduced in (14). Its modal component $V_p(x)$ can be obtained by retaining only the residue contribution in $k_x = k_{xp}$ of (14) as follows:

$$V_p(x) = -j\,\frac{2}{\mathbb{D}'(k_{xp})}\, e^{-jk_{xp}x}. \tag{22}$$

The expression of the electric current flowing in the inner conductor of the CPW can be derived as the circulation around the

inner conductor of the y-component of the magnetic field, radiated by the magnetic currents. This leads to the following expression for the total electric current:

$$I(x) = \sum_{i=1}^{2} \int_{-(w_i/2)}^{+(w_i/2)} \frac{1}{4\pi^2} \int_{-\infty}^{+\infty} \int_{-\infty}^{+\infty} \mathbb{V}(k_x) J_0\left(k_y \frac{w}{2}\right) \cdot \frac{2j \sin(k_y d) k_x k_y e^{-jk_x x} e^{-jk_y y}}{k_0 \zeta_0 \sqrt{k_i^2 - k_x^2 - k_y^2}} \, dk_x \, dk_y \, dy \quad (23)$$

where $w_i = 2d - w$ is the inner conductor width and $\mathbb{V}(k_x)$ is the FT of $V(x)$. Capturing again only the pole contribution to the integrals in k_x of (23), we obtain

$$I_p(x) = V_p(x) \frac{jk_{xp}}{\pi k_0 \zeta_0} \sum_{i=1}^{2} \int_{-\infty}^{+\infty} \frac{J_0\left(k_y \frac{w}{2}\right) \sin(k_y d) k_y}{\sqrt{k_i^2 - k_{xp}^2 - k_y^2}} \cdot \int_{-(w_i/2)}^{+(w_i/2)} e^{-jk_y y} \, dy \, dk_y. \quad (24)$$

We can now express the characteristic admittance of the CPW as

$$Y_0 = \frac{I_p(x)}{V_p(x)} = \frac{jk_{xp}}{\pi k_0 \zeta_0} \sum_{i=1}^{2} \int_{-\infty}^{+\infty} \frac{J_0\left(k_y \frac{w}{2}\right) \sin(k_y d) k_y}{\sqrt{\tilde{k}_{ip}^2 - k_y^2}} \cdot \int_{-(w_i/2)}^{+(w_i/2)} e^{-jk_y y} \, dy \, dk_y \quad (25)$$

where $\tilde{k}_{ip} = \sqrt{k_i^2 - k_{xp}^2}$ and $\mathrm{Im}[\tilde{k}_{ip}] < 0$ for $i = 1$ and $\mathrm{Im}[\tilde{k}_{ip}] > 0$ for $i = 2$. By performing the integration in y, substituting, as before, (17) and (18) in (25) and inverting again the order of the space and spectral integrations, we finally obtain the following expression for the characteristic admittance:

$$Y_0 = \sum_{i=1}^{2} \frac{2k_{xp}}{j\pi k_0 \zeta_0 w} \left[\int_{2d-w}^{2d} \frac{H_0^2(\tilde{k}_{ip}|y|)}{\sqrt{1 - \frac{4\left(2d - \frac{w}{2} - y\right)^2}{w^2}}} \, dy - \int_0^w \frac{H_0^2(\tilde{k}_{ip}|y|)}{\sqrt{1 - \frac{4\left(\frac{w}{2} - y\right)^2}{w^2}}} \, dy \right]. \quad (26)$$

ACKNOWLEDGMENT

The authors wish to thank R. Wyss, currently with Aleph Lightgate Corporation, Monrovia, CA, for having performed part of the measurements presented in this paper. This work was carried out at the Jet Propulsion Laboratory, California Institute of Technology, Pasadena.

REFERENCES

[1] B. S. Karasik, M. C. Gaidis, W. R. McGrath, B. Bumble, and H. G. LeDuc, "Low noise in a diffusion-cooled hot-electron mixer at 2.5 THz," *Appl. Phys. Lett.*, vol. 71, p. 1567, 1997.

[2] W. F. M. Gonzeules, J. R. Gao, W. M. Laauwen, G. de Lange, T. M. Klapwijlc, and P. A. J. del Corte, "Direct and heterodyne response of quasioptical Nb hot electron bolometer mixers designed for 2.5 THz radiation detection," in *Proc. 11th Int. Space Terahertz Technol. Symp.*, Ann Arbor, MI, May 2000, pp. 69–81.

[3] D. B. Rutledge, D. P. Neikirk, and D. P. Kasiligan, "Infrared and millimeter-waves," in *Integrated Circuit Antennas*, K. J. Button, Ed. New York: Academic, 1983, vol. 10, pp. 1–90.

[4] D. F. Filippovic, S. S. Gearhart, and G. M. Rebeiz, "Double-slot antennas on extended hemispherical and elliptical silicon dielectric lenses," *IEEE Trans. Microwave Theory Tech.*, vol. 41, pp. 1738–1749, Oct. 1993.

[5] J. Kawamura, T. Hunter, C.-Y. E. Tong, R. Blundell, D. C. Papa, F. Patt, W. Peters, T. Wilson, C. Henkel, G. Gol'tsman, and E. Gershenzon, "Ground-based terahertz spectroscopy toward Orion," *Astron. and Astrophys. Lett.*, Dec. 2002, to be published.

[6] M. Van der Vorst, P. J. I. De Maagt, A. Neto, A. Reynolds, W. Luinge, R. Heres, and M. Herben, "Effect of the internal reflection on the radiation properties and input impedance of integrated lens antennas: Comparisons between theory and measurements," *IEEE Trans. Microwave Theory Tech.*, vol. 49, pp. 1118–1125, June 2001.

[7] R. A. Wyss, A. Neto, W. R. McGrath, B. Bumble, and H. LeDuc, "Submillimeter-wave spectral response of twin-slot antennas coupled to hot electron bolometers," in *Proc. 11th Int. Space Terahertz Technol. Symp.*, Solid-State Electron. Lab., Univ. of Michigan at Ann Arbor, MI, May 1–3, 2000, J. East, Ed., pp. 379–388.

[8] A. Neto, P. J. I. De Maagt, and S. Maci, "Optimized basis functions for slot antennas excited by coplanar waveguides," *IEEE Trans. Antennas Propagat.*, June 2003, to be published.

[9] J.-H. Son, H.-H. Wang, J. F. Whitaker, and G. A. Mourou, "Picosecond pulse propagation on coplanar striplines fabricated on lossy semiconductor substrates: Modeling and experiments," *IEEE Trans. Microwave Theory Tech.*, vol. 41, pp. 1574–1580, Sept. 1993.

[10] D. R. Jackson, F. Mesa, M. J. Freire, D. P. Nyquist, and C. Di Nallo, "An excitation theory for bound modes and residual-wave currents on stripline structures," *Radio Sci.*, vol. 35, no. 2, pp. 495–510, Mar.–Apr. 2000.

[11] A. Neto and S. Maci, "Green's function of an infinite slot printed between two homogeneous dielectric. Part I: Magnetic currents," *IEEE Trans. Antennas Propagat.*, June 2003, to be published.

[12] N. K. Das, "A new theory of the characteristic impedance of general printed transmission lines applicable when power leakage exists," *IEEE Trans. Microwave Theory Tech.*, vol. 48, pp. 1108–1117, July 2000.

[13] K. C. Gupta, *Microstrip Lines and Slotlines*, R. Garg and I. J. Bahl, Eds. Norwood, MA: Artech House, 1979.

[14] A. Neto and S. Maci, "Input impedance of an infinite slot printed between two homogeneous dielectric," Jet Propulsion Lab., Pasadena, CA, JPL Internal Rep. D/21 322, 2000.

[15] A. Neto and P. H. Siegel, "Equivalent network characterization for series fed microstrip lines on thin slabs," *IEEE Trans. Microwave Theory Tech.*, submitted for publication.

[16] D. Pasqualini and S. Maci, "High frequency improvements to PO-based methods for the analysis of integrated dielectric lens antennas," presented at the 32nd Eur. Microwave Conf., Milan, Italy, Sept. 23–27, 2002.

Paolo Focardi received the Doctor and Ph.D. degrees in electronic engineering from the University of Florence, Florence, Italy, in 1998 and 2002, respectively.

In 1998, he joined the Department of Electronics and Telecommunications, University of Florence, in collaboration with the Italian Space Agency. His research concerns the analysis of large arrays of rectangular horn and slot antennas for space applications. From 1999 to 2000, he was a member of the Operative Italian Scientific Team involved in the Shuttle Radar Topography Mission (SRTM). In 2001, he was a Visiting Researcher with the Sub-Millimeter Wave Superconductive Sensors Group, Jet Propulsion Laboratory, California Institute of Technology, Pasadena, where he was involved with HEB-based mixers for deep-space observation at terahertz frequencies. In 2002, he joined the Sub-Millimeter Wave Superconductive Sensors Group, Microwave Experiment Systems and Technology Section, Jet Propulsion Laboratory, California Institute of Technology. His research is focused on analytical and numerical methods in electromagnetics with particular emphasis on the acceleration of mutual coupling integrals.

Andrea Neto received the Doctor degree (*cum laude*) from the University of Florence, Florence, Italy, in 1994, and the Ph.D. degree from the University of Siena, Siena, Italy, in 2000, both in electronic engineering.

He spent almost three years with the Antenna Section, European Space Agency (ESA) Research and Technology Center (ESTEC). Since February 2000 to August 2001, he has been with the Sub-Millimeter Wave Advanced Technology Group, Jet Propulsion Laboratory, California Institute of Technology, Pasadena. Since October 2001, he has been with FEL–TNO, Den Haag, The Netherlands. His research is focused on analytical and numerical methods in electromagnetics, with emphasis on the analysis of large arrays and integrated circuits and antennas.

William R. McGrath (M'88) received the B.S. degree in physics from the Massachusetts Institute of Technology (MIT), Cambridge, in 1978, and the M.A. and Ph.D. degrees in physics from the University of California at Berkeley, in 1981 and 1985, respectively.

From 1980 to 1987, his research focused on the device physics of superconductor–insulator–superconductor (SIS) mixers and superconductive circuits. He and his coworkers were the first to measure the quantum effects of large-gain and quantum-limited noise in SIS mixers at millimeter wavelengths. From 1985 to 1987, he was a Visiting Researcher with the Chalmers University of Technology, Göteborg, Sweden, where he was involved with submillimeter-wave superconductive detectors. He and his coworkers built the first millimeter-wave Josephson effect mixer using newly discovered Hi-Tc superconductors. In 1987, he joined the staff of the Jet Propulsion Laboratory, California Institute of Technology, Pasadena, where he is currently a Senior Research Scientist and Group Supervisor with the Microwave Experiment Systems and Technology Section. He heads a research group that develops superconductive HEB mixers and direct detectors for terahertz remote-sensing applications. He has authored or co-authored over 160 publications in this field.